Inorganic Chemistry

Article

pubs.acs.org/IC

# Network Flexibility: Control of Gate Opening in an Isostructural Series of Ag-MOFs by Linker Substitution

Marcel Handke,[†] Hanna Weber,[†] Marcus Lange,[‡] Jens Möllmer,[‡] Jörg Lincke,[†] Roger Gläser,[‡] Reiner Staudt,[§] and Harald Krautscheid*,[†]

[†]Fakultät für Chemie und Mineralogie, Universität Leipzig, Johannisallee 29, 04103 Leipzig, Germany

[‡]Institut für Nichtklassische Chemie e.V., Permoserstraße 15, 04318 Leipzig, Germany

[§]Fakultät Maschinenbau und Verfahrenstechnik, Hochschule Offenburg, Badstraße 24, 77652 Offenburg, Germany

Supporting Information

**ABSTRACT:** An isostructural series of 15 structurally flexible microporous silver metal−organic frameworks (MOFs) is presented. The compounds with a dinuclear silver core as secondary building unit ($Ag_2N_4$) can be obtained under solvothermal conditions from substituted triazolyl benzoate linkers and $AgNO_3$ or $Ag_2SO_4$; they exhibit 2-fold network interpenetration with **lvt** topology. Besides the crystal structures, the calculated pore size distributions of the microporous MOFs are reported. Simultaneous thermal analyses confirm the stability of the compounds up to 250 °C. Interconnected pores result in a three-dimensional pore structure. Although the porosity of the novel coordination polymers is in the range of only 20−36%, this series can be regarded as a model system for investigation of network flexibility, since the pore diameters and volumes can be gradually adjusted by the substituents of the 3-(1,2,4-triazol-4-yl)-5-benzamidobenzoates. The pore volumes of selected materials are experimentally determined by nitrogen adsorption at 77 K and carbon dioxide adsorption at room temperature. On the basis of the flexible behavior of the linkers a reversible framework transformation of the 2-fold interpenetrated network is observed. The resulting adsorption isotherms with one or two hysteresis loops are interpreted by a gate-opening process. Due to external stimuli, namely, the adsorptive pressure, the materials undergo a phase transition confirming the structural flexibility of the porous coordination polymer.

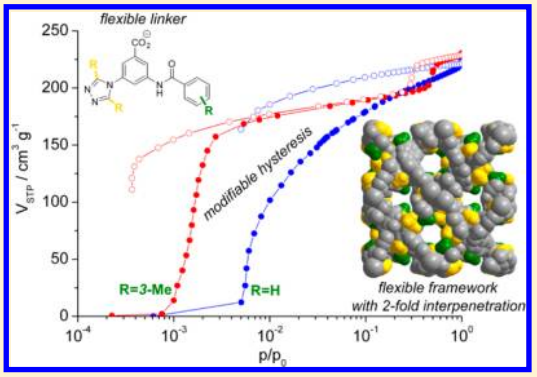


## INTRODUCTION

Metal−organic frameworks (MOFs) or porous coordination polymers (PCPs) have gained increasing interest in the last decades because of their distinct adsorption properties and high diversity of possible framework structures.[1] As highly porous materials, MOFs possess great potential for applications in gas separation and storage,[2] as sensors,[3] in heterogeneous catalysis,[4] and in thermal energy storage.[5] The potential of MOFs forming highly ordered porous structures has been impressively shown by the synthesis of, for example, the well-known HKUST-1[6] and MOF-5[7] as well as the MIL[8] and DUT[9] series. In addition to the frequently investigated pure carboxylates, nitrogen-containing heterocycles such as pyridines, pyrazoles, triazoles, and tetrazoles were found to be valuable ligands in the synthesis of MOFs because of their tunable coordination behavior.[10] Regarding the different behavior of MOFs during the activation procedure, the materials are classified according to Kitagawa in three generations.[11] Typical for structurally flexible MOFs, stepwise adsorption−desorption isotherms are noticeable. Such flexible materials reveal a so-called gate-opening process in which the framework undergoes a structural transformation along with a sudden increase in adsorption capacity.[11,12] The phenomenon of structural flexibility is a response to external stimuli such as pressure or temperature.[13] With substituted triazolyl benzoates containing anionic carboxylate and neutral 1,2,4-triazole donor groups[14] porous and structurally flexible copper-based MOFs have already been reported.[15]

Herein we report on an isostructural series of 15 structurally flexible microporous Ag-MOFs with 2-fold network interpenetration and closely related linkers whereupon we obtained three types of crystallographically related structures. In contrast to the most common **dia** topology[16,17] especially for interpenetrated frameworks,[18] the isostructural frameworks reported here are described with the point symbol $\{4^2.8^4\}$ and the less common topology type **lvt**, first reported for MOFs by Boldog et al.[19]

Based on 15 substituted 3-(1,2,4-triazol-4-yl)-5-benzamidobenzoate ligands ($\mathbf{L1^-}$−$\mathbf{L15^-}$), the pore diameters and volumes of the isostructural Ag-MOFs **1**−**15** (Table 1) can be gradually adjusted. The ligands bear substituents with different sterical

**Received:** April 22, 2014

   dx.doi.org/10.1021/ic500908r | *Inorg. Chem.* XXXX, XXX, XXX−XXX

Table 1. Linker Substitution Pattern of the Isostructural Ag-MOFs $_\infty^3[Ag_2(L)_2]$ (1−15)

| | $R^1$ | $R^2$ | $R^3$ | structure type | | $R^1$ | $R^2$ | $R^3$ | structure type |
|---|---|---|---|---|---|---|---|---|---|
| $L1^-$ | Me | Me | H | II | $L8^-$ | Me | Et | H | I |
| $L2^-$ | Me | Me | 3-Me | III | $L9^-$ | Me | Et | 3-Me | III |
| $L3^-$ | Me | Me | 4-Me | III | $L10^-$ | Me | Et | 4-Me | III |
| $L4^-$ | Me | Me | 3,5-$Me_2$ | III | $L11^-$ | Me | Et | 3,5-$Me_2$ | III |
| $L5^-$ | Me | Me | 3-OMe | III | $L12^-$ | Me | Et | 3-OMe | III |
| $L6^-$ | Me | Me | 4-OMe | III | $L13^-$ | Me | Et | 4-OMe | III |
| $L7^-$ | Me | Me | 3,5-$(OMe)_2$ | III | $L14^-$ | Me | Et | 3,5-$(OMe)_2$ | III |
| | | | | | $L15^-$ | Et | Et | H | I |

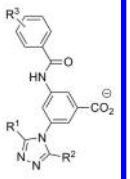

Table 2. Unit Cells of 1−5 and 8−15.

| | 1 | 2 | 3 | 4 | 5 | 8 |
|---|---|---|---|---|---|---|
| structure type | II | III | III | III | III | I |
| space group | $I4_1/acd$ | $Iba2$ | $Iba2$ | $Iba2$ | $Iba2$ | $I4_1/acd$ |
| lattice constant [pm] | $a$ = 2873.7(3) | $a$ = 2340.7(5) | $a$ = 2329.18(6) | $a$ = 2330.24(5) | $a$ = 2321.49(8) | $a$ = 2856(1) |
| | | $b$ = 2954.5(6) | $b$ = 2715.41(8) | $b$ = 2932.23(8) | $b$ = 2756.6(1) | |
| | $c$ = 6940(1) | $c$ = 2917.1(6) | $c$ = 3104.0(1) | $c$ = 2970.87(9) | $c$ = 3029.1(1) | $c$ = 2303.9(9) |
| volume [$10^6$ pm$^3$] | 57308(12) | 20174(7) | 19632(1) | 20299.4(9) | 19384(1) | 18788(15) |
| $Z$ | 48 | 16 | 16 | 16 | 16 | 16 |

| 9 | 10 | 11 | 12 | 13 | 14 | 15 |
|---|---|---|---|---|---|---|
| III | III | III | III | III | III | I |
| $Iba2$ | $Iba2$ | $Iba2$ | $Iba2$ | $Iba2$ | $Iba2$ | $I4_1/acd$ |
| $a$ = 2318.95(8) | $a$ = 2332.85(7) | $a$ = 2339.87(6) | $a$ = 2323.72(6) | $a$ = 2299.14(8) | $a$ = 2333.5(8) | $a$ = 2866.1(2) |
| $b$ = 2964.5(2) | $b$ = 2799.2(1) | $b$ = 2823.29(8) | $b$ = 2850.6(1) | $b$ = 2975.8(1) | $b$ = 3037(1) | $c$ = 2297.8(1) |
| $c$ = 2951.6(1) | $c$ = 3083.7(1) | $c$ = 3081.2(1) | $c$ = 2971.6(1) | $c$ = 2878.8(1) | $c$ = 2734(3) | |
| 20291(2) | 20137(1) | 20355(1) | 19684(1) | 19696(2) | 19375(21) | 18875(2) |
| 16 | 16 | 16 | 16 | 16 | 16 | 16 |

demand, i.e., hydrogen, methyl, ethyl, and methoxy, at different positions, and the size of the pores that are interconnected to a three-dimensional pore structure depends on the linker substituents. Therefore, this series of MOFs allows investigation of the influence of linker substituents on the gate-opening behavior.

Besides the single-crystal structures, powder X-ray diffraction (PXRD), temperature-dependent PXRD, thermogravimetry/mass spectrometry (TG-MS) data, and adsorption properties with $N_2$ and $CO_2$ as adsorptives are discussed.

## X-RAY CRYSTALLOGRAPHY

The coordination polymers **1**−**15** were obtained by solvothermal synthesis from either $Ag_2SO_4$ or $AgNO_3$ and H(**L1**)−H(**L15**) in $H_2O$/MeCN (1:1, v/v). The detailed syntheses are available in the Supporting Information. The crystal structures of **1**−**5** and **8**−**15** were determined by X-ray diffraction. The crystals of compounds **1**, **2**, **8**, and **14** exhibited only a low scattering power using a laboratory X-ray source (Mo K$\alpha$, $\lambda$ = 71.073 pm). Therefore, the crystal structure analyses were performed using synchrotron radiation ($\lambda$ = 82.657 pm) at the beamline 14.2 of the synchrotron source BESSY-II.[20,21]

The differences in the linker substituents lead to different crystal symmetry. **1**, **8**, and **15** crystallize in the centrosymmetric tetragonal space group $I4_1/acd$ (no. 142), whereas **2**−**7** and **9**−**14** crystallize in the noncentrosymmetric orthorhombic space group $Iba2$ (no. 45). Nevertheless, the crystal structures are closely related to each other, and the structural relationships correlate to a group−subgroup relationship of the space groups.[22] $I4_1/acd$ (**8**, **15**; structure type **I**) has a maximal isomorphic subgroup with the lowest index of three $I4_1/acd$ with $c' = 3c$ (**1**; structure type **II**), resulting in a three times larger unit cell (Table 2). Since $Iba2$ (**2**−**7**, **9**−**14**; structure type **III**) is a nonisomorphic subgroup of $Ibca$, $I4_1cd$, and $I\bar{4}c2$, and $I4_1/acd$ again is a nonisomorphic supergroup of these space groups, the structural relationship is confirmed (Figure S3).[22] The crystallographic $c$ axis of **1**, **8**, and **15** corresponds to the crystallographic $a$ axis of **2**−**7** and **9**−**14**. According to the group−subgroup relationship, the contents of the asymmetric unit increase from half a formula unit $[Ag_2(L)_2]$ in **8** and **15** (structure type **I**) to one and a half units in **1** (structure type **II**) and two units in **2**−**5** and **9**−**14** (structure type **III**), respectively. Representatively for the isostructural MOFs, the crystal structures[23] of compounds **1**, **4**, and **8** are discussed in the following.

The silver atoms in the crystal structures of **1**, **4**, and **8** are monodentately coordinated by two triazole groups and one carboxylate group (Figure 1). Thus, the coordination of each silver atom results in a trigonal planar $N_2O_1$ coordination (bond lengths and bond angles for **1**, **4**, and **8** are given in Table 3). The out-of-plane distances of the silver atoms are in the range 1.0(5)−29.2(4) pm for **1**, 4.9(1)−15.4(1) pm for **4**, and 8.1(1) pm for **8** caused by weak coordinative interactions of the second carboxylate oxygen atoms (e.g., distance range for **4**: 268.4(3)−281.6(4) pm). In each case two silver atoms are bridged by two triazole groups to dinuclear $Ag_2N_4$ rings as


dx.doi.org/10.1021/ic500908r | Inorg. Chem. XXXX, XXX, XXX−XXX

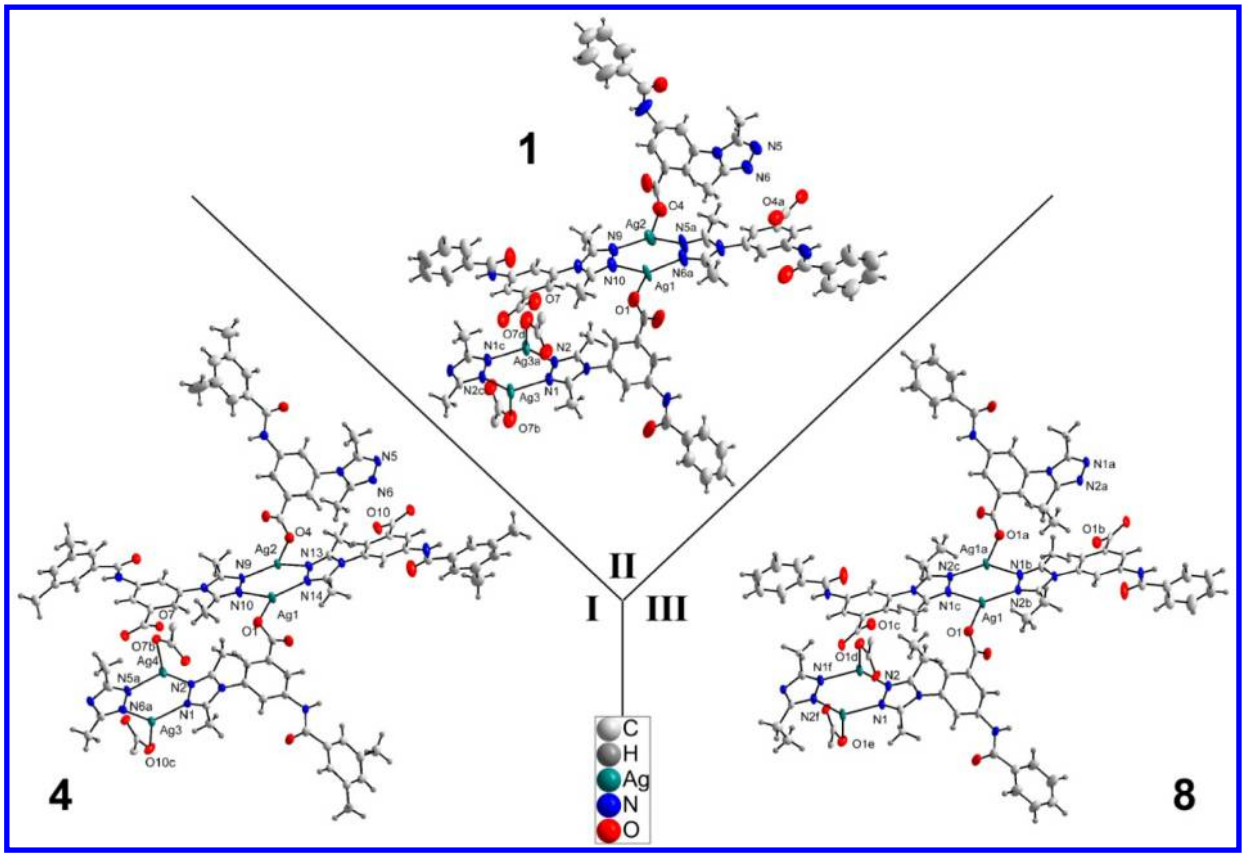


**Figure 1.** Fragments of the crystal structures of **1**, **4**, and **8** (50% ellipsoids). **I**, **II**, and **III** label the structure types.

**Table 3. Selected Bond Lengths and Angles of 1, 4, and 8**[a]

| 1 | | 4 | | 8 | |
|---|---|---|---|---|---|
| | bond length [pm] | | bond length [pm] | | bond length [pm] |
| Ag1–N6a | 222.6(7) | Ag1–N14 | 222.0(4) | Ag1–N2b | 219.1(3) |
| Ag1–N10 | 225.7(6) | Ag1–N10 | 225.3(4) | Ag1–N1c | 226.7(3) |
| Ag1–O1 | 230.4(7) | Ag1–O1 | 234.2(4) | Ag1–O1 | 228.3 (3) |
| Ag2–N9 | 225.6(5) | Ag2–N9 | 220.6(3) | | |
| Ag2–N5a | 219.1(5) | Ag2–N13 | 225.2(3) | | |
| Ag2–O4 | 221.8(6) | Ag2–O4 | 232.5(3) | | |
| Ag3–N2c | 220.4(4) | Ag3–N6a | 221.6(4) | | |
| Ag3–N1 | 225.2(4) | Ag3–N1 | 225.0(3) | | |
| Ag3–O7b | 231.7(5) | Ag3–O10c | 231.9(4) | | |
| | | Ag4–N2 | 220.0(3) | | |
| | | Ag4–N5a | 224.7(4) | | |
| | | Ag4–O7b | 235.7(3) | | |
| | bond angle [deg] | | bond angle [deg] | | bond angle [deg] |
| N10–Ag1–N6a | 125.6(2) | N10–Ag1–N14 | 126.1(1) | N1c–Ag1–N2b | 125.7(1) |
| O1–Ag1–N6a | 134.3(3) | O1–Ag1–N14 | 132.9(1) | O1–Ag1–N2b | 131.9(1) |
| O1–Ag1–N10 | 100.1(2) | O1–Ag1–N10 | 100.8(1) | O1–Ag1–N1c | 102.0(1) |
| N9–Ag2–N5a | 123.7(2) | N9–Ag2–N13 | 123.4(1) | | |
| O4–Ag2–N9 | 128.9(2) | O4–Ag2–N9 | 130.6(1) | | |
| O4–Ag2–N5a | 104.9(2) | O4–Ag2–N13 | 104.6(1) | | |
| N1–Ag3–N2c | 119.5(1) | N1–Ag3–N6a | 124.1(1) | | |
| O7b–Ag3–N2c | 132.7(1) | O10c–Ag3–N6a | 128.9(1) | | |
| O7b–Ag3–N1 | 107.8(2) | O10c–Ag3–N1 | 106.4(1) | | |
| | | N2–Ag4–N5a | 123.1(1) | | |
| | | O7b–Ag4–N2 | 136.2(1) | | |
| | | O7b–Ag4–N5a | 100.4(1) | | |

[a]Symmetry codes for **1**: a: 0.25+*y*, 1.75−*x*, 1.25−*z*; b: 1−*x*, 1.5−*y*, *z*; c: 1−*x*, 2−*y*, 1−*z*. Symmetry codes for **4**: a: 0.5+*x*, −0.5+*y*, −0.5+*z*; b: 2−*x*, *y*, −0.5+*z*; c: 1.5−*x*, −0.5+*y*, *z*. Symmetry codes for **8**: a: 1.5−*x*, 1.5−*y*, 1.5−*z*; b: 0.25+*y*, 1.25−*x*, −0.25+*z*; c: 1.25−*y*, 0.25+*x*, 1.75−*z*.


dx.doi.org/10.1021/ic500908r | *Inorg. Chem.* XXXX, XXX, XXX–XXX

structural motifs. The distances between the silver atoms in the $Ag_2N_4$ ring units are 341.0(6)−362.8(1) pm in **1**, 344.6(1)−348.4(1) pm in **4**, and 342.3(1) pm in **8**. Whereas the dinuclear triazole-bridged silver units represent four-connected nodal points, the ligands operate as two-connected bridges, resulting in **lvt** topology[24] with the point symbol $\{4^2.8^4\}$. The resulting four- and eight-membered rings are responsible for the formation of two different cavities (Figure 2). Viewing along the crystallographic *c*-direction two pore windows with diameters of 400 and 300 pm are visible in **1** as presented in Figure 3. The diameters of both pore windows in **8** are 300 pm, whereas in the crystal structure of **4** the equivalent pore windows are 300 and 250 × 200 pm (viewed along the *a*-direction). The networks possess a 2-fold interpenetration of type **IIa** with 2-fold rotation axes as full interpenetration symmetry elements (FISE for **1**, **8**: 2[1,0,0], 2[0,1,0], 2[1,−1,0]; FISE for **4**: 2[0,0,1]).[17,24] The remaining solvent-accessible pore volume[25] of the three-dimensional networks amounts to 36% in **1**, 34% in **4**, and 32% in **8**. As shown in Figure 3, the substituents on the triazole and benzoyl rings are oriented toward the cavities. Comparing **1**, **4**, and **8** it is obvious that the introduction of methyl groups to the benzoyl ring ($\mathbf{L4}^-$) and the sterically demanding ethyl group on the triazole ring ($\mathbf{L8}^-$) reduces the network porosity. The pore size distributions are discussed in detail below.

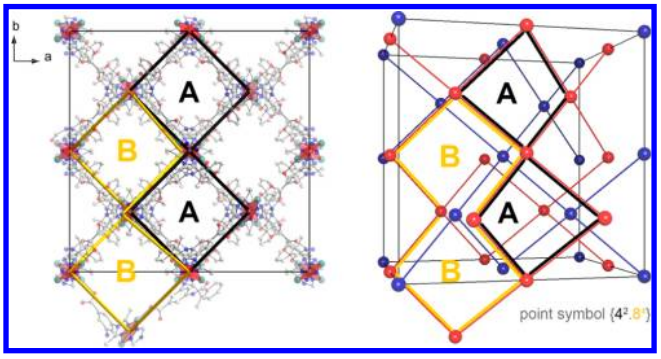


**Figure 2.** Left: Representation of the unit cell of **8** with **lvt** topology,[24] point symbol $\{4^2.8^4\}$ (H atoms are omitted). $Ag_2N_4$ units are emphasized in red, black lines represent the four-membered rings, and yellow lines represent an eight-membered ring. Right: Perspective view of simplified networks of **8** with two interpenetrated nets (red and blue) with view along [−105]. The four-membered rings create the pore labeled A, whereas the eight-membered rings create pore B.

## PORE SIZE DISTRIBUTION

Figure 4 shows the calculated pore size distributions (PSD) of **1**−**5** and **8**−**15** based on their crystal structure data.[26,27] In general, the PSDs show significant differences in their appearances, caused by the substituents of the 1,2,4-triazole and benzoyl groups that are oriented toward the cavities (Figure 3, Figure S6). This result is consistent with the IRMOF concept,[28] in which both pore size and shape can be influenced by the choice of ligands with different sterical requirement. As expected, compound **1**, bearing ligand $\mathbf{L1}^-$ with the lowest sterical demand, has the largest pore diameter of up to 670 pm. But the diameters of the most frequent pores of **1** are around 580 and 520 pm. By introduction of an ethyl group on the triazole ring, the diameter of the most frequent pores is reduced by 50 pm (520 pm in **8**). With a second ethyl substituent on the triazole ring this pore diameter decreases again to 470 pm (**15**).

Introduction of a substituent in *meta* position of the benzoyl group leads to a shift of the diameter of the most frequent

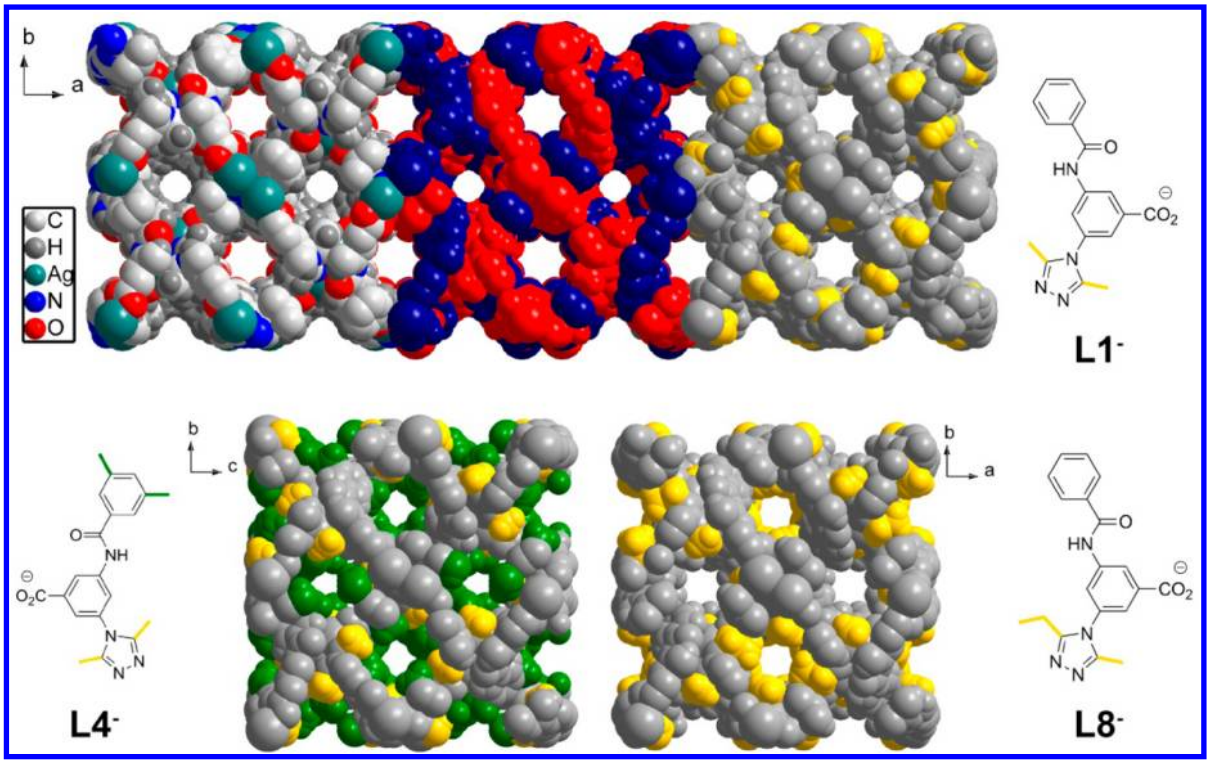


**Figure 3.** Space-filling diagrams of **1** (top), **4** (bottom left), and **8** (bottom right). Two interpenetrated nets (top center) and the position of the substituents (yellow, green) are emphasized.


dx.doi.org/10.1021/ic500908r | Inorg. Chem. XXXX, XXX, XXX−XXX

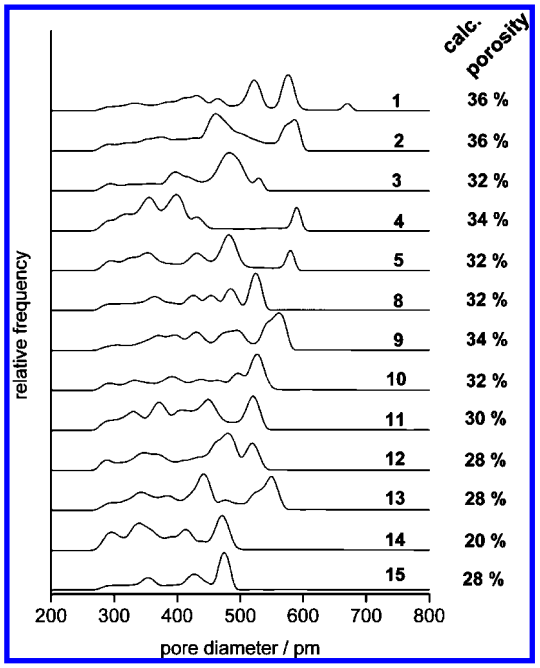


**Figure 4.** Pore size distribution[26,27] and porosity[25] of **1**−**5** and **8**−**15** calculated from single-crystal structure data.

pores to 460 and 590 pm for **2** and to 480 and 580 pm for **5**. A second substituent on the benzoyl group shifts the diameters of these cavities to about 400 and 590 pm (**4**). In contrast to **2**, **4**, and **5**, which still show pore sizes up to 590 pm, **3**, with a methyl group in *para* position of the benzoyl group, has the most abundant and largest cavities in the range of 450 and 530 pm. In this case $\mathbf{L3}^-$ seems to realize a complete blocking of pore sizes between 540 and 580 pm. However, in the case of **8**−**14** different positions of the ethyl groups at the triazole ring can lead to differences in the orientations into the pores. This results in two limiting forms of possible PSDs (Figures S4 and S5). In general the frameworks **8**−**15** with the ethyl-substituted triazole ligands show their maxima at smaller pore diameters between 450 and 550 pm.

## X-RAY POWDER DIFFRACTION

Phase purity is confirmed by comparison of the X-ray powder diffraction patterns with the simulated powder patterns based on single-crystal data (Figure 5, Figures S8−S10). As a representative example for the isostructural MOFs, **1** is discussed in detail. Both the positions and the intensities of the reflections of the air-dried product agree with those of the simulated patterns. After Soxhlet extraction with methanol over 7 days and air drying, **1** has the same structure as the material obtained by solvothermal synthesis. However, after vacuum activation and after $CO_2$ and $N_2$ sorption experiments, a completely different powder diffraction pattern was observed for **1** at room temperature, indicating a phase transition. After resolvation with methanol, the original powder diffraction pattern of **1** is restored. The framework connectivity is maintained, but its crystal structure changes due to the external stimulus.[29]

While single-crystal structures of compounds **1**−**5** and **8**−**15** could be determined from single-crystal diffraction data, **6** and **7** could be identified by X-ray powder diffraction. The similarity of the PXRD data shown in Figure 6 confirms the presence of the isostructural framework series. The compounds crystallize

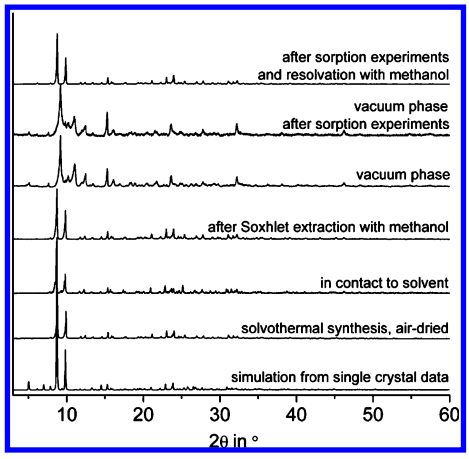


**Figure 5.** X-ray powder diffraction patterns ($\lambda$(Cu K$\alpha_1$) = 154.060 pm) of **1** obtained by solvothermal synthesis and after postsynthetic treatments in comparison to the simulated X-ray powder diffraction pattern based on single-crystal data.

in three different structure types. Furthermore, all presented MOFs have the same topology (**lvt**, point symbol $\{4^2.8^4\}$) in which the dinuclear triazole-bridged silver units are connected by the substituted 3-(1,2,4-triazol-4-yl)-5-benzamidobenzoate ligands. The differences in the unit cells, structures, and symmetry lead to differences in the positions of the reflections (Figure 6). In the case of the tetragonal structures **1**, **8**, and **15** (structure types **I** and **II**) the single *206* or *202* reflections correspond to reflections *202* and *220* in the orthorhombic compounds **2**−**7** and **9**−**14** (structure type **III**), caused by different lengths of the lattice constants *a* and *b*. This correlation is shown in detail in Figure S11.

It is to be noted that the single crystals of compounds **1**−**15** are breaking apart while drying in air. However, the PXRD measurements confirm that the dried powder sample is still crystalline. It is likely that the loss of solvent at room temperature induces a phase transition (Figure S8−S10).

## THERMAL STABILITY

In Figure 7 the temperature-dependent X-ray powder diffraction pattern (TD-PXRD) of **1** is shown. The compound undergoes a phase transition at 120 °C, which is associated with the elimination of water ($m/z$ = 18), confirmed in the TG-DTA-MS analysis of **1** (Figure 8). The resulting phase decomposes at about 250 °C. Above the decomposition temperature the formation of elemental silver is detected. A first TG-DTA-MS measurement of **1** was carried out with a Soxhlet-extracted (MeOH), dry sample after vacuum activation. This sample does not show a mass loss up to the decomposition temperature. A second air-dried sample was measured without any activation. Up to 120 °C a mass loss of 5.5% was found, which correlates with the calculated weight loss for about three water molecules (5.7%). The decomposition of **1** starting at 250 °C is endothermic and takes place under release of carbon dioxide ($m/z$ = 44).

## SORPTION STUDIES

Sorption measurements of compounds **1**, **2**, **4**, **5**, **8**, **9**, **12**, **13**, and **15** were performed with nitrogen at 77 K and carbon dioxide at 298 K. The obtained isotherms are illustrated in Figure 9 ($CO_2$) and Figure 10 ($N_2$). These isotherms do not fit to the recommended IUPAC classification[30] because of a


dx.doi.org/10.1021/ic500908r | Inorg. Chem. XXXX, XXX, XXX−XXX

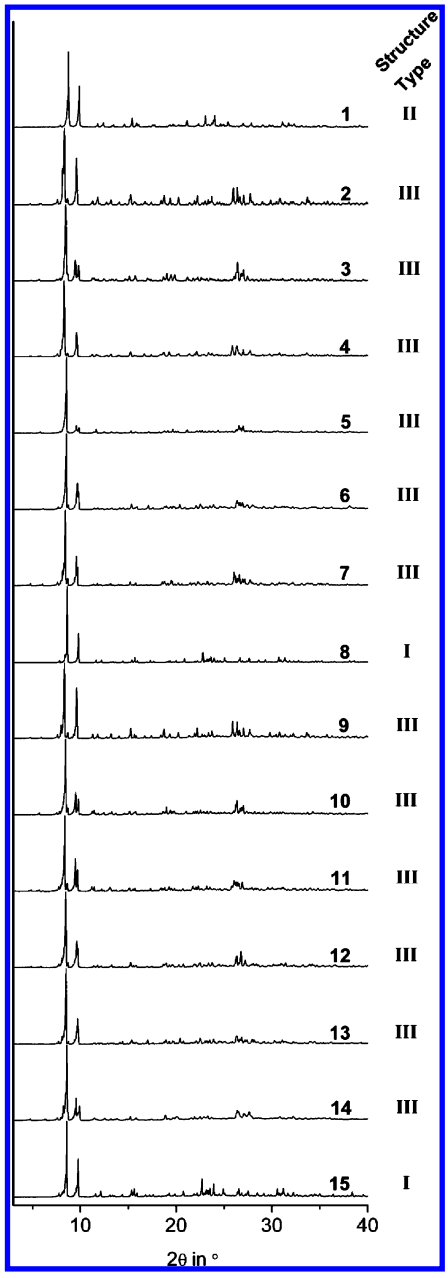


**Figure 6.** X-ray powder diffraction patterns ($\lambda$(Cu K$\alpha_1$) = 154.060 pm) of **1**−**15** in contact with $H_2O$/MeCN (1:1, v/v).

reproducible (Figure S14−S22) stepwise pore filling and a sigmoidal curvature in logarithmic scale. In particular, low carbon dioxide loadings (<2 mmol $g^{-1}$) in the low-pressure region (<0.64 MPa) are followed by a sudden steep increase at a specific pressure, known as the gate-opening pressure.[31−34] In addition, desorption branches confirm this sorption behavior, which is typical for flexible MOF materials.[11,29] For the investigated network compounds different gate-opening pressures are observed depending on the substitution pattern of the ligand. Fischer et al. also observed a relation between substitution of the linker and gate-opening pressure.[32,33] Sorption studies on functionalized $[Zn_2(bdc)_2(dabco)]_n$ materials, which offer flexibility by introduction of alkyl ether groups on the ligand, show that these groups act as molecular gates[32] for guest molecules and thus control the sorption behavior.

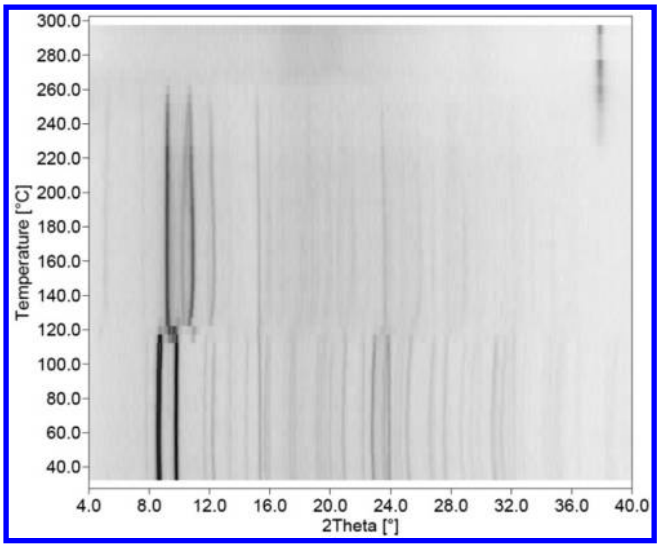


**Figure 7.** Temperature-dependent X-ray powder diffraction patterns ($\lambda$(Cu K$\alpha_1$) = 154.060 pm) (Guinier−Simon diagram) of **1**.

In this study substituents constrict the pore apertures. As a consequence, the pore diameter can be tuned. We expect that the linkers **L1**$^-$−**L15**$^-$ present in **1**−**15** have enough degrees of freedom for reversible rotation and bending, which is important for the expansion or shrinkage of the networks. On the basis of this flexible nature of **L1**$^-$−**L15**$^-$ a reversible framework transformation is observed. We assume that the 2-fold network interpenetration in **1**−**15** further supports structural framework flexibility, leading to hysteresis of the sorption isotherm for $CO_2$ and $N_2$ for **1**−**15**. Interpenetrated networks have been shown to form open and closed phases by interdigitation using a glide movement.[34] Thus, the various substituents on the triazole and benzoyl ring with their orientation toward the cavities (Figures S6, S7) and their different sterical demand are able to influence this network movement and can affect both the gate-opening pressure and the shape of the hysteresis loop (Figures 9 and 10).

It becomes obvious that substitution with ethyl groups on the triazole ring does not affect the gate-opening pressure for carbon dioxide sorption too much (Figure 9a); for **1**, **8**, and **15** the gate-opening pressure is in a very close range between 0.43 and 0.64 MPa, although the materials show different sorption capacities for the first sorption step before gate-opening. The structural change depends on the external pressure for these materials. A small additional step is observed for **8** with a hysteresis loop at $p$ = 0.02−0.2 MPa. On the other hand, by introduction of methyl or methoxy groups on the benzoyl ring the gate-opening pressure decreases (Figure 9b,c) for carbon dioxide sorption at 298 K from 0.64 MPa for **1** without any methyl group, to 0.16 MPa for **2** with one and 0.23 MPa for **4** with two methyl groups on the benzoyl ring (Figure 9b). This might be a consequence of stronger interactions of $CO_2$ and the contracted pore walls of the evacuated material. If the methyl group is replaced by a methoxy group, the gate opening is slightly shifted to higher pressures, from 0.16 MPa for **2** to 0.3 MPa for **5** (Figure 9d). Again, the introduction of an ethyl group on the triazole ring does not influence the gate-opening pressure.

Moreover, substitution influences the pore volume in sorption measurements. In particular, by substitution of the triazole ring the pore volume decreases from 0.33 $cm^3$ $g^{-1}$ for **1**


dx.doi.org/10.1021/ic500908r | Inorg. Chem. XXXX, XXX, XXX−XXX

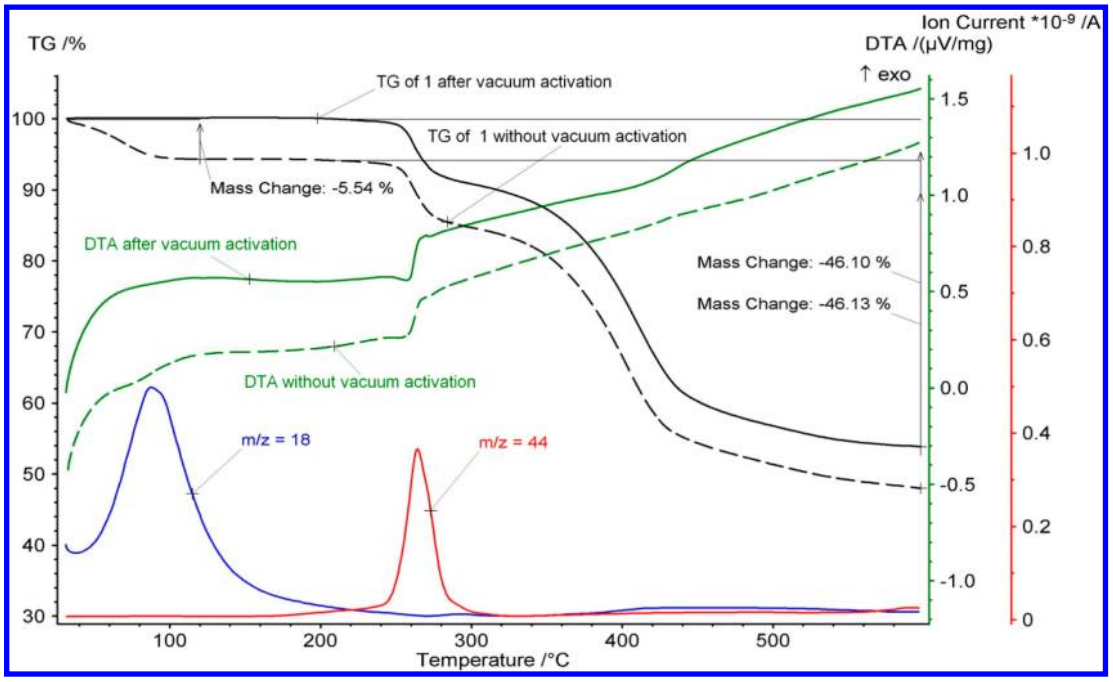


**Figure 8.** TG-DTA-MS analysis of **1** with and without previous activation under vacuum. The black traces represent the thermogravimetry (TG) signals, while the green lines represent the differential thermal analysis (DTA), and the blue and red traces show the mass spectrometry (MS) signals.

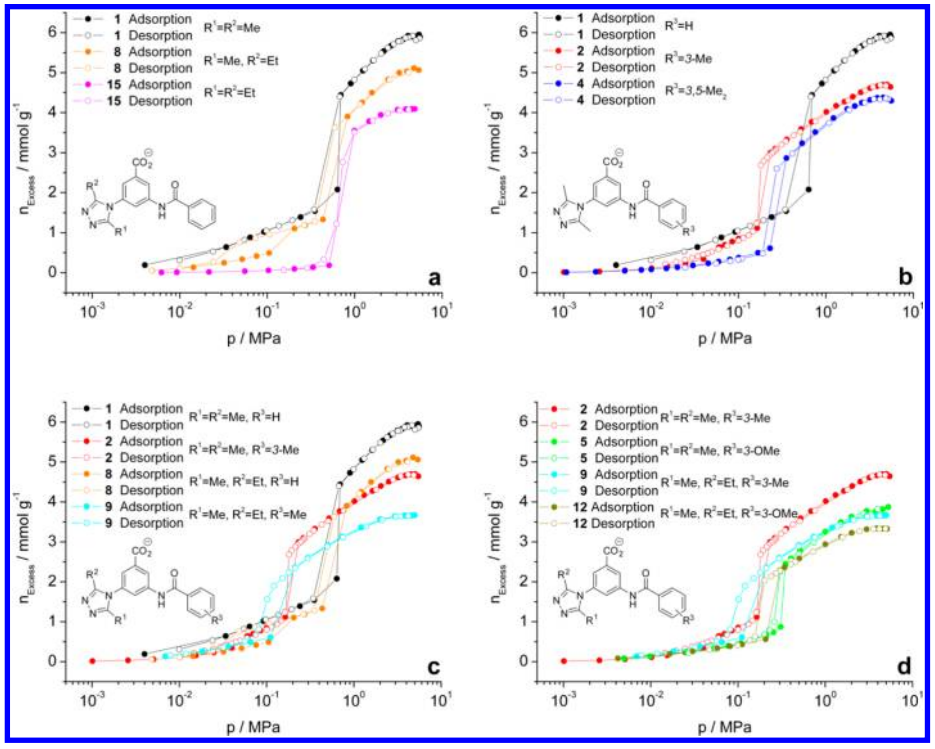


**Figure 9.** Carbon dioxide sorption isotherms (298 K, closed symbols adsorption, open symbols desorption) for compounds **1**, **2**, **4**, **5**, **8**, **9**, **12**, and **15**. Influence of different substituents at the triazole group (a), at the benzoyl group (b), and variation of methyl and ethyl substitution on triazole and different *meta* substitutions at the benzoyl ring (c, d).

to 0.28 $cm^3\ g^{-1}$ for **8** with one and 0.22 $cm^3\ g^{-1}$ for **15** with two ethyl groups (Figure 9a). The same effect is found if the benzoyl ring is methylated (Figure 9c, **2** and **9**). Similarly, the pore volume decreases with introduction of methyl or methoxy groups on the benzoyl ring.

The nitrogen sorption isotherms (77 K) also show a stepwise pore filling with low loadings up to a certain pressure, after which a steep increase is observed. In contrast to $CO_2$ (298 K), the $N_2$ sorption isotherms reveal large hysteresis loops in the low-pressure region, typical for structurally flexible MOFs. In case of **2**, **4**, **5**, and **8** an additional step can be observed at low relative pressures ($p/p_0 > 0.0005$ for **4**, $p/p_0 > 0.07$ for **8**, $p/p_0 >$ 0.4 for **2** and **5**).


dx.doi.org/10.1021/ic500908r | *Inorg. Chem.* XXXX, XXX, XXX−XXX

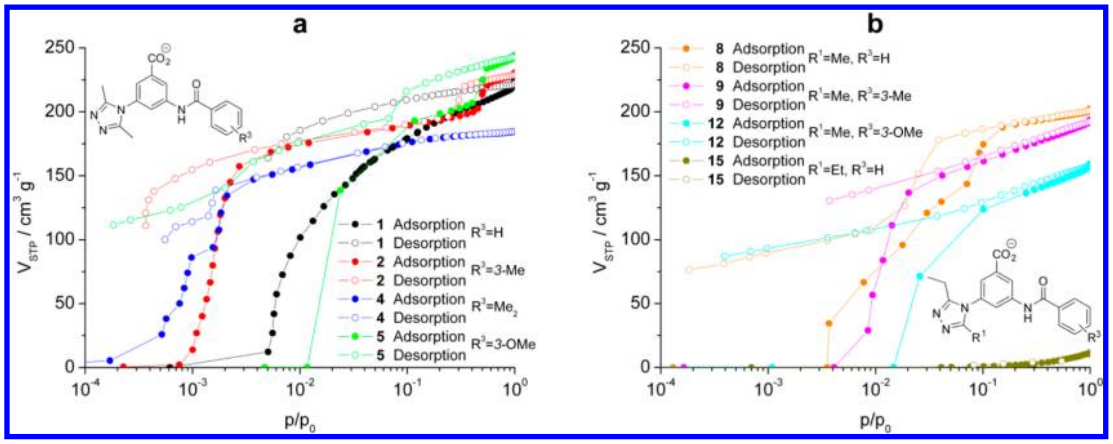


**Figure 10.** Nitrogen sorption isotherms (77 K, $p_0$ = 0.0972 MPa, closed symbols adsorption, open symbols desorption) of compounds **1**, **2**, **4**, **5**, **8**, **9**, **12**, and **15**. Representation of sorption isotherms of compounds with methyl- (a) and ethyl-substituted triazoles (b).

Again, the sorption isotherm curvature is influenced by substitution of the triazole and benzoyl ring of the linker. The introduction of one (**8**) or two ethyl groups (**15**) on the triazole ring causes a decrease in pore volume, particularly for **15** with almost no nitrogen adsorbed. The ethyl groups with higher sterical demand lead to smaller pore diameters. However, **15** is a porous material shown by carbon dioxide sorption, but nitrogen sorption at 77 K is kinetically hindered. This observation is consistent with the calculated PSD shown in Figure 4 with pore diameters smaller than 500 pm. The modification on the benzoyl ring affects the sorption isotherm shape more drastically. In particular, by introduction of methoxy or methyl groups in *meta* position the sorption isotherms offer a multistepwise pore filling: one methyl (**2**) or methoxy group (**5**) in *meta* position presents an additional gate opening ($p/p_0$ > 0.4). Similarly, for **4** with two methyl groups on the benzoyl ring, an additional gate-opening step appears at low relative pressure ($0.0005 \leq p/p_0 \leq 0.002$). Furthermore, the methyl and methoxy groups reduce the pore volume ($p/p_0$ = 0.3). But, in contrast, at higher pressures ($p/p_0$ > 0.4) additional transitions lead to higher pore volume compared to unsubstituted materials.

Obviously the sterical demand of a substituent in *meta* position of the benzoyl group causes a further framework transformation, and the structure changes into an energetically more favored form. However, this structural transformation seems to be hindered by an additional sterically demanding ethyl group on the triazole ring or another substituent on the benzoyl group. Thus, compounds **2** and **5** show a second hysteresis loop at higher pressures caused by the *meta* substitution.

## CONCLUSION

The Ag-based MOFs **1**−**15** form an isostructural series with **lvt** topology and a thermal stability up to 250 °C. **1**−**15**, obtained under solvothermal conditions, consist of two interpenetrated three-dimensional networks formed from the 3-(1,2,4-triazol-4-yl)-5-benzamidobenzoates and dinuclear $Ag_2N_4$ ring units as secondary building units. Their pore diameters and pore volumes can be adjusted by linker substituents, and the calculated porosity of **1**−**15** is in the range between 20% and 36%. The calculated PSDs of the microporous MOFs show some essential differences in their appearances, caused by the substituents of the 1,2,4-triazole and benzoyl groups that are oriented toward the cavities. The pore volumes of several selected materials are determined by nitrogen adsorption measurements at 77 K, resulting in a maximum pore volume of up to 0.38 cm$^3$ g$^{-1}$ (49%) for **5**. The adsorption studies with nitrogen and carbon dioxide demonstrate the high flexibility of the new materials, and the sorption experiments result in isotherms with one or two hysteresis loops. The variations of the sterical demand of the substituent of the triazole and the benzoyl group adjust the pore volume to 0.18−0.33 cm$^3$ g$^{-1}$ for carbon dioxide and 0.20−0.38 cm$^3$ g$^{-1}$ for nitrogen. **1**−**15** with their 2-fold network interpenetration and structural flexibility form a series of isostructural MOFs suitable for systematic studies of the influence of linker substitution on network porosity and gate-opening behavior.

## ASSOCIATED CONTENT

### Supporting Information

Experimental details of ligand and MOF syntheses, detailed characterization by X-ray diffraction, thermal analyses, calculated pore size distribution, IR spectroscopy, adsorption measurements, as well as scanning electron microscopy. This material is available free of charge via the Internet at http://pubs.acs.org. CCDC 995524−995528, 996077−996080, and 996084−996087 contain the supplementary crystallographic data. These data can be obtained free of charge from the Cambridge Crystallographic Data Centre via www.ccdc.cam.ac.uk/data_request/cif.

## AUTHOR INFORMATION

### Corresponding Author

*E-mail: Krautscheid@rz.uni-leipzig.de.

### Notes

The authors declare no competing financial interest.

## ACKNOWLEDGMENTS

The Helmholtz-Zentrum Berlin (BESSY-II) is acknowledged for granting beam time and travel support, in particular, Dr. U. Müller and his team for assistance during data collection. Diffraction data have been collected on BL14.2 operated by the Joint Berlin MX-Laboratory at the BESSY II electron storage ring (Berlin-Adlershof, Germany). We thank D. Hirsch and D. Poppitz (Leibniz-Institut für Oberflächenmodifizierung e.V.) for recording SEM images. We gratefully acknowledge financial support by Deutsche Forschungsgemeinschaft (DFG SPP 1362, Poröse metallorganische Gerüstverbindungen, STA 428/17-2,

KR 1675/7-2, and GL290/6-2) and ESF. M.H. and J.L. are grateful for ESF fellowships. This work was funded by the European Union and the Free State of Saxony. We thank the Universität Leipzig (PbF-1) and the graduate school BuildMoNa.

## REFERENCES

(1) (a) Janiak, C.; Vieth, J. K. *New J. Chem.* **2010**, *34*, 2366−2388. (b) Furukawa, H.; Ko, N.; Go, Y. B.; Aratani, N.; Choi, S. B.; Choi, E.; Yazaydin, A. Ö.; Snurr, R. Q.; O'Keeffe, M.; Kim, J.; Yaghi, O. M. *Science* **2010**, *329*, 424−428. (c) Mondal, S.; Bhunia, A.; Kelling, A.; Schilde, U.; Janiak, C.; Holdt, H. *J. Am. Chem. Soc.* **2014**, *136*, 44−47.

(2) (a) Hartmann, M.; Kunz, S.; Himsl, D.; Tangermann, O.; Ernst, S.; Wagener, A. *Langmuir* **2008**, *24*, 8634−8642. (b) D'Alessandro, D. M.; Smit, B.; Long, J. R. *Angew. Chem., Int. Ed.* **2010**, *49*, 6058−6082. (c) Debatin, F.; Thomas, A.; Kelling, A.; Hedin, N.; Bacsik, Z.; Senkovska, I.; Kaskel, S.; Junginger, M.; Müller, H.; Schilde, U.; Jäger, C.; Friedrich, A.; Holdt, H.-J. *Angew. Chem., Int. Ed.* **2010**, *49*, 1258−1262. (d) Mondal, S.; Dey, S.; Baburin, I.; Kelling, A.; Schilde, U.; Seifert, G.; Janiak, C.; Holdt, H. *CrystEngComm* **2013**, *15*, 9394−9399.

(3) (a) Harbuzaro, B. V.; Corma, A.; Rey, F.; Atienzar, P.; Jordá, J. L.; García, H.; Ananias, D.; Carlos, L. D.; Rocha, J. *Angew. Chem., Int. Ed.* **2008**, *47*, 1080−1083. (b) Bauer, C. A.; Timofeeva, T. V.; Settersten, T. B.; Patterson, B. D.; Liu, V. H.; Simmons, B. A.; Allendorf, M. D. *J. Am. Chem. Soc.* **2007**, *129*, 7136−7144.

(4) Corma, A.; Garcia, H.; Llabres, F. X.; Xamena, I. *Chem. Rev.* **2010**, *110*, 4606−4655.

(5) (a) Henninger, S. K.; Habib, H. A.; Janiak, C. *J. Am. Chem. Soc.* **2009**, *131*, 2776−2777. (b) Jeremias, F.; Khutia, A.; Henninger, S. K.; Janiak, C. *J. Mater. Chem.* **2012**, *22*, 10148−10151. (c) Janiak, C.; Henninger, S. K. *Chimia* **2013**, *67*, 419−424.

(6) Chui, S. S.-Y.; Lo, S. M.-F.; Charmant, J. P. H.; Orpen, A. G.; Williams, I. D. *Science* **1999**, *83*, 1148−1150.

(7) Li, H.; Eddaoudi, M.; O'Keeffe, M.; Yaghi, O. M. *Nature* **1999**, *402*, 276−279.

(8) Férey, G.; Mellot-Draznieks, C.; Serre, C.; Millange, F.; Dutour, J.; Surblé, S.; Margiolaki, I. *Science* **2005**, *309*, 2040−2042.

(9) (a) Kleine, N.; Senkovska, I.; Gedrich, K.; Stoeck, U.; Henschel, A.; Mueller, U.; Kaskel, S. *Angew. Chem., Int. Ed.* **2009**, *48*, 9954−9957. (b) Kleine, N.; Herzog, C.; Sabo, M.; Senkovska, I.; Getzschmann, J.; Paasch, S.; Lohe, M.; Brunner, E.; Kaskel, S. *Phys. Chem. Chem. Phys.* **2010**, *12*, 11778−11784. (c) Gedrich, K.; Senkovska, I.; Kleine, N.; Stoeck, U.; Henschel, A.; Lohe, M.; Baburin, I.; Mueller, U.; Kaskel, S. *Angew. Chem., Int. Ed.* **2010**, *49*, 8489−8492. (d) Grünker, R.; Senkovska, I.; Biedermann, R.; Kleine, N.; Lohe, M.; Müller, P.; Kaskel, S. *Chem. Commun.* **2011**, *47*, 490−492. (e) Hauptvogel, I.; Biedermann, R.; Kleine, N.; Senkovska, I.; Cadiau, A.; Wallach, D.; Feyerherm, R.; Kaskel, S. *Inorg. Chem.* **2011**, *50*, 8367−8374.

(10) (a) Haasnoot, G. *Coord. Chem. Rev.* **2000**, *200*, 131−185. (b) Habib, A.; Sanchiz, J.; Janiak, C. *Dalton Trans.* **2008**, *13*, 1734−1744. (c) Lysenko, A. B.; Govor, E. V.; Krautscheid, H.; Domasevitch, K. V. *Dalton Trans.* **2006**, *31*, 3772−3776. (d) Lincke, J.; Lässig, D.; Stein, K.; Moellmer, J.; Kuttatheyil, A. V.; Reichenbach, C.; Moeller, A.; Staudt, R.; Kalies, G.; Bertmer, M.; Krautscheid, H. *Dalton Trans.* **2012**, *41*, 817−824. (e) Mondal, S.; Bhunia, A.; Kelling, A.; Schilde, U.; Janiak, C.; Holdt, H. *Chem. Commun.* **2014**, *50*, 5441−5443.

(11) (a) Kitagawa, S.; Kondo, M. *Bull. Chem. Soc. Jpn.* **1998**, *71*, 1739−1753. (b) Kitagawa, S.; Kitaura, R.; Noro, S. *Angew. Chem., Int. Ed.* **2004**, *43*, 2334−2375.

(12) Li, D.; Kaneko, K. *Chem. Phys. Lett.* **2001**, *335*, 50−56.

(13) (a) Kitaura, R.; Seki, K.; Akiyama, G.; Kitagawa, S. *Angew. Chem., Int. Ed.* **2003**, *42*, 428−431. (b) Serre, C.; Millange, F.; Thouvenot, C.; Nogues, M.; Marsolier, G.; Louer, D.; Férey, G. *J. Am. Chem. Soc.* **2002**, *124*, 13519−13526. (c) Serre, C.; Bourrelly, S.; Vimont, A.; Ramsahye, N. A.; Maurin, G.; Llewellyn, P. L.; Daturi, M.; Filinchuk, Y.; Leynaud, O.; Barnes, P.; Férey, G. *Adv. Mater.* **2007**, *19*, 2246−2251. (d) Llewellyn, P. L.; Horcajada, P.; Maurin, G.; Devic, T.; Rosenbach, N.; Bourrelly, S.; Serre, C.; Vincent, D.; Loera-Serna, S.; Filinchuk, Y.; Férey, G. *J. Am. Chem. Soc.* **2009**, *131*, 13002−13008. (e) Mondal, S.; Bhunia, A.; Baburin, I.; Jäger, C.; Kelling, A.; Schilde, U.; Seifert, G.; Janiak, C.; Holdt, H. *Chem. Commun.* **2013**, *49*, 7559−7601.

(14) Lässig, D.; Lincke, J.; Krautscheid, H. *Tetrahedron Lett.* **2010**, *51*, 653−656.

(15) (a) Lincke, J.; Lässig, D.; Moellmer, J.; Reichenbach, C.; Puls, A.; Moeller, A.; Gläser, R.; Kalies, G.; Staudt, R.; Krautscheid, H. *Microporous Mesoporous Mater.* **2011**, *142*, 62−69. (b) Lässig, D.; Lincke, J.; Moellmer, J.; Reichenbach, C.; Moeller, A.; Gläser, R.; Kalies, G.; Cychosz, K. A.; Thommes, M.; Staudt, R.; Krautscheid, H. *Angew. Chem., Int. Ed.* **2011**, *50*, 10344−10348.

(16) Batten, S. R.; Neville, S. M.; Turner, D. R. *Coordination Polymers - Design, Analysis and Application*; RSC Publishing: Cambridge, U.K., 2009.

(17) (a) Blatov, V. A.; Carlucci, L.; Ciani, G.; Proserpio, D. M. *CrystEngComm* **2004**, *6*, 377−395. (b) Baburin, I. A.; Blatov, V. A.; Carlucci, L.; Ciani, G.; Proserpio, D. M. *J. Solid State Chem.* **2005**, *178*, 2452−2474.

(18) Alexandrov, E. V.; Blatov, V. A.; Kochetkov, A. V.; Proserpio, D. M. *CrystEngComm* **2011**, *13*, 3947−3958.

(19) Boldog, I.; Rusanov, E. B.; Chernega, A. N.; Sieler, J.; Domasevitch, K. V. *J. Chem. Soc., Dalton Trans.* **2001**, 893−897.

(20) Mueller, U.; Darowski, N.; Fuchs, M. R.; Förster, R.; Hellmig, M.; Paithanker, K. S.; Pühringer, S.; Steffien, M.; Zocher, G.; Weiss, M. S. *J. Synchrotron Radiat.* **2012**, *19*, 442−449.

(21) Krug, M.; Weiss, M. S.; Heinemann, U.; Mueller, U. *J. Appl. Crystallogr.* **2012**, *45*, 568−572.

(22) (a) Hahn, T. *International Tables of Crystallography*, Volume A, Section 7. (b) Shmueli, U. *International Tables of Crystallography*, Volume B, Section 2.4. (c) Authier, A. *International Tables of Crystallography*, Volume D, Section 3.3.

(23) Sheldrick, G. M. *Acta Crystallogr.* **2008**, *A64*, 112−122.

(24) *TOPOS* 4.0: Blatov, V. A. *IUCr CompComm Newsletter* **2006**, *7*, 4−8; http://www.topos.ssu.samara.ru.

(25) *PLATON*: Spek, A. L. *J. Appl. Crystallogr.* **2003**, *36*, 7−13.

(26) (a) Gelb, L. D.; Gubbins, K. E. *Langmuir* **1999**, *15*, 305−308. (b) Bhattacharya, S.; Gubbins, K. E. *Langmuir* **2006**, *22*, 7726−7731. (c) Bhattacharya, S. *PSDsolv*; http://supriyo.net/research/psd/psd.htm.

(27) Schmiedel, P. *PSDres*; Universität Leipzig, 2011.

(28) Eddaoudi, M.; Kim, J.; Rosi, N.; Vodak, D.; Wachter, J.; O'Keeffe, M.; Yaghi, O. M. *Science* **2002**, *295*, 469−472.

(29) Kitagawa, S.; Uemura, K. *Chem. Soc. Rev.* **2005**, *34*, 109−119.

(30) Sing, K. S. W.; Everett, D. H.; Haul, R. A. W.; Mouscou, L.; Pierotti, R. A.; Rouquerol, J.; Siemieniewska, T. *Pure Appl. Chem.* **1985**, *57*, 603−619.

(31) Li, D.; Kaneko, K. *Chem. Phys. Lett.* **2001**, *335*, 50−56.

(32) Henke, S.; Schmid, R.; Grunwaldt, J.-D.; Fischer, R. A. *Chem.—Eur. J.* **2010**, *16*, 14296−14306.

(33) Henke, S.; Schneemann, A.; Wütscher, A.; Fischer, R. A. *J. Am. Chem. Soc.* **2012**, *134*, 9464−9474.

(34) (a) Chen, B.; Liang, C.; Yang, J.; Contreras, D. S.; Clancy, Y. L.; Lobkovsky, E. B.; Yaghi, O. M.; Dai, S. *Angew. Chem., Int. Ed.* **2006**, *45*, 1390−1393. (b) Horike, S.; Shimomura, S.; Kitagawa, S. *Nat. Chem.* **2009**, *1*, 695−704. (c) Bureekaew, S.; Sato, H.; Matsuda, R.; Kubota, Y.; Hirose, R.; Kim, J.; Kato, K.; Takata, M.; Kitagawa, S. *Angew. Chem., Int. Ed.* **2010**, *49*, 7660−7664. (d) Takashima, Y.; Martínez, V. M.; Furukawa, S.; Kondo, M.; Shimomura, S.; Uehara, H.; Nakahama, M.; Sugimoto, K.; Kitagawa, S. *Nat. Commun.* **2011**, *2*, 168.